PROCEEDINGS OF SCIENCE

Centaurus A: Hard X-ray and high-energy gamma-ray light curve correlation

Isak D. Davids*
North-West University, Centre for Space Research, Private Bag X6001, Potchefstroom 2520, South Africa, and
University of Namibia, Private Bag 13301, Department of Physics, Windhoek, Namibia, 12010
E-mail: isak.davids@gmail.com

Markus Böttcher
North-West University, Centre for Space Research, Private Bag X6001, Potchefstroom 2520, South Africa
E-mail: Markus.Bottcher@nwu.ac.za

Michael Backes
University of Namibia, Private Bag 13301, Department of Physics, Windhoek, Namibia, 12010
and
North-West University, Centre for Space Research, Private Bag X6001, Potchefstroom 2520, South Africa E-mail: mbackes@unam.na

Centaurus A (Cen A), powered by a 55 million solar mass supermassive black hole, has been intensively monitored in all accessible wavelength ranges of the electromagnetic spectrum. However, its gamma-ray flux, both in the H.E.S.S. very-high and the *Fermi*-LAT high-energy gamma-ray regimes, is relatively faint, hampering light curve analyses. Yet, the extensive long-term light curve data from *Fermi*-LAT and *Swift*-BAT (hard X-rays) allows for cross-correlation studies. We find a hint that X-ray emission from Cen A precedes the gamma rays by 25 days. If this lag is real and related to a gamma-gamma absorption effect in the *broad-line region* (BLR) around the central source, then we can constrain the size of the BLR using light-travel time arguments. These are first results of extended light curve correlation studies between high-energy gamma rays and X-rays from Cen A.

5th Annual Conference on High Energy Astrophysics in Southern Africa
4-6 October 2017
University of the Witwatersrand (Wits), South Africa

*Speaker.

PoS(HEASA2017)010

Abbreviations

The following abbreviations are frequently used in this manuscript:

BAT	**B**urst **A**lert **T**elescope (on-board Neil Gehrels *Swift* Observatory)
BLR	**B**road **L**ine **R**egion
DCF	**D**iscrete **C**orrelation **F**unction
HE	**H**igh-**E**nergy (gamma rays of energy $\sim 0.1 - 100$ GeV)
H.E.S.S.	**H**igh-**E**nergy **S**tereoscopic **S**ystem
IACT	**I**maging **A**tmospheric **C**herenkov **T**elescope
LAT	**L**arge **A**rea **T**elescope (on-board Fermi satellite)
RG	**R**adio **G**alaxy
SED	**S**pectral **E**nergy **D**istribution
VHE	**V**ery **H**igh-**E**nergy (gamma rays of energy $\gtrsim 100$ GeV)

1. Introduction

Radio Galaxies (RGs) belong to the type of *active galactic nuclei* (AGN) for which the jet viewing angle with respect to our line of sight is relatively large in contrast to *blazars* for which this angle is small. A well-studied near-by radio galaxy is *Centaurus A* (Cen A). These sources are in general featuring a broadband (from radio to γ-rays) emission spectrum which is primarily attributed to non-thermal radiation. Two distinct peaks can be seen in such a *spectral energy distribution* (SED) where the lower energy peak (extending from radio to X-rays) is traditionally accepted as being due to *synchrotron emission* from relativistic electrons from the jet. The second hump (from X-rays to γ-rays) in the SED is attributed to inverse-Compton upscattering of a soft target photon field by the same relativistic jet electrons.

Amongst the basic components of the structure of a typical AGN, are the fast-moving high-density clouds surrounding the central engine (but external to the jet) and located closer to the central *super-massive black hole* (SMBH) than the optically obscuring dust torus. Due to the broad emission lines from this region, observed in the optical, these components are referred to as the *broad line regions* (BLRs) of the AGN. The location of the BLR can be measured by the *reverberation method* employing the *light travel time* in conjunction with the observable temporal lag in different energy band emission. The intense BLR radiation field is likely to be an efficient target photon field for $\gamma\gamma$-absorption producing electron-positron (e^-e^+) pairs [1, 2]. On the other hand, most of the X-ray emission from AGN arises from the inner regions around the SMBH (see e.g. [3]).

In this work, we report results from a discrete cross-correlation of light curves as applied to *Swift*-BAT X-ray and *Fermi*-LAT γ-ray long-term observations of the nearest radio galaxy, Cen A.

2. Centaurus A

The massive elliptical galaxy NGC 5128 (discovered in 1826), is the closest radio galaxy (often referred to as Cen A), at a distance of 3.4 Mpc [4]. This source is centrally powered by a SMBH of mass 5.5×10^7 $M_\odot$ (see e.g. [5, 6]). The radio lobes of Cen A subtend $\sim 10^\circ$ on the sky, due to both their gigantic sizes and the proximity of the source to Earth. Cen A is a Fanaroff-Riley Type I radio galaxy [7]. The source has been observed from radio to *very-high energy* (VHE; $E \gtrsim 100$ GeV) γ-rays, and is an ideal target for studying radio lobes and relativistic outflows.

Numerous extensive studies have so far been carried out on Cen A, aiming at characterizing the SED of the source. A break in the γ-ray spectrum of the source above 2.4 GeV has been established [8]. This break is not well modeled using a leptonic synchrotron self-Compton model. Recent results, from a joint initiative by H.E.S.S. and *Fermi*-LAT [9], show that the VHE data points are consistently above the *high-energy* (HE; $E \sim 0.1 - 100$ GeV) power-law extrapolation of the γ-ray spectrum measured below the break. There is clear evidence for a second spectral component in VHE γ-rays in the SED.

As part of the aforementioned studies, various theoretical models with different emission mech-

anisms and particle populations are usually employed to describe the SED of Cen A, as shown in Figure 1.

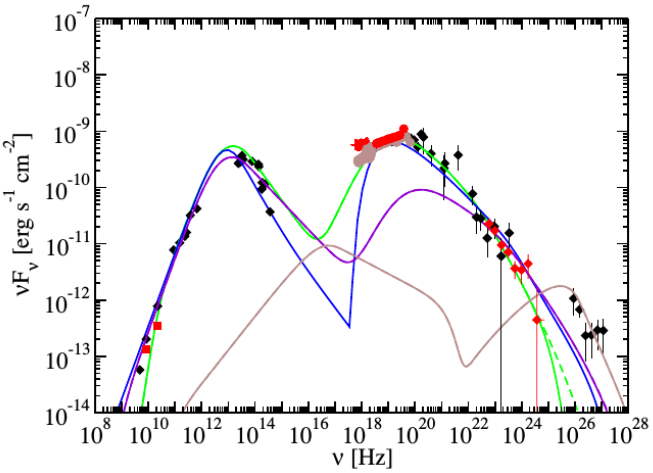

Figure 1: The broad band SED of the core of Cen A depicting numerous observations with model fits described in [10]. The symbols are observational data points: these are VLBI (red squares), *Swift*-XRT (red crosses), *Suzaku* X-rays (brown circles), *Swift*-BAT (red circles), *Fermi*-LAT (red diamonds), H.E.S.S. and other archival data (black symbols). The green model fits *synchrotron self-Compton* emission, while removing $\gamma\gamma$ absorption from the latter produces the dashed green curve. The violet curve is a fit that attempts to account for the highest energy gamma rays, while the brown curve attempts to fit the H.E.S.S. data. Considering the possibility of a decelerating relativistic outflow [11] produces the blue fit.

The data points in Figure 1 range from radio (at the lowest energy regime) to the VHE γ-rays at the highest energy part. The red circles at the peak of the second hump show the X-ray data from *Swift*-XRT[1]. The red diamonds depicting the HE γ-rays are obtained from the *Fermi*-LAT. As can be seen in Figure 1, various models successfully reproduce and fit the large part of the observed multi-wavelength data, characterizing the SED of Cen A. The first peak is generally associated with synchrotron emission from relativistic electrons, while second peak in the HE regime is explained using leptonic and hadronic models. In the one-zone leptonic case (shown in green in the SED), γ-rays are produced by the upscattering of low energy photons by the relativistic electrons through the inverse-Compton process by a single emission region (typically a spherical blob) traveling at relativistic speed along the jet. These target low energy photon populations can be internal or external to the jet system. Such a single-zone SSC (also used for various blazars) is usually popular to describe this component. Also shown by others, e.g. [12] and also evident from Figure 1, one can invoke a second emission zone (here shown in brown) with differing input parameters to account for the VHE data points. These two-zone scenario has been recently employed by the *Fermi*-LAT and H.E.S.S. collaborations to fully explain the entire γ-ray of the SED of Cen A.

Alternatively (for AGN in general), the hadronic explanation of the HE peak uses energetic protons (interacting with low-energy photons) that produce γ-rays after photo-pion production that leads to

[1] *Swift*-XRT is the *X-Ray Telescope* also on board *Swift* for measuring the fluxes, spectra, and light curves of GRBs sensitive in the $0.2-10$ keV band.

pion and muon decay processes (or from proto-synchrotron radiation). These hadronic models will typically require an input of rather large power in the proton population (see e.g. [13]) reaching $10^{47} - 10^{49}$ erg $\cdot$ s^{-1}. The corresponding luminosity estimates are much lower, by even 2 or more orders of magnitude for leptonic models — this essentially attributed to electrons radiating more efficiently.

A combination of leptonic and hadronic (leptohadronic) models have also been used in successful reproduction of the HE tail of the SED of Cen A where the TeV component is considered as an emission from relativistic proton population that interacts with the photons (photohadronic interaction) produced by the primary leptonic component [12]. Another nearby radio galaxy, *IC* 310 (which features a double-peak structure up to a few GeV) is another example where photohadronic interactions explains the observed GeV through TeV spectra [14].

It could be that $\gamma\gamma$-absorption might give an indication of this component, and indeed $\gamma\gamma$ absorption in the BLR of *blazars* has been considered by several authors (see e.g. [15, 1, 2]) who reported that significant $\gamma\gamma$ absorption by the BLR can be avoided by having the γ-ray emission region outside the BLR.

3. Multi-wavelength Observations

To study the long-term activity of Cen A, we obtained contemporary data spanning about 6.8 years of hard X-rays and high-energy γ-rays. In addition to these, VHE γ-ray emission was probed for any variability.

The main factor that drove the specific data selection was the pressing need of contemporaneous data with the H.E.S.S. (High-Energy Stereoscopic System) observatory [16, 17]. The next subsections describe these observations briefly.

3.1 VHE γ-ray Data

Long-term TeV γ-ray data were obtained from H.E.S.S., one of the current ground-based *Imaging Atmospheric Cherenkov Telescopes* (IACTs). These data spanned the period from 2004 till 2011 — the period in which the system operated as H.E.S.S. Phase I. In these phase, the system with four 12 m IACTs (each of 108 m^2 mirror area) arranged in form of a square of side-length of 120 m. Unfortunately, these quiescent state observations of Cen A in the TeV band resulted in a rather low-significance light curve not allowing meaningful light curve correlation analysis with other wavebands.

No data where included from the H.E.S.S. Phase II period when the system had an additional 28 m telescope (with mirror area amounting to 614 m^2) added.

3.2 X-ray Data

Hard X-ray data (15 $-$ 150 keV) from the *Burst Alert Telescope* (BAT)[18] on board the Swift observatory was used to obtain a 6.8 year span light curve. While primarily designed for *gamma-*

ray burst (GRB) detection and rapid triggering, BAT is an efficient hard X-ray monitor instrument [19], releasing "Swift/BAT transient monitor results provided by the Swift/BAT team" [20]. These data are readily available from the BAT transient source online repository[2], and have been used to produce the light curve binned in 14 day bins in the period from MJD 54703.6 to MJD 57195.6 (i.e. between 8 August, 2008 and 22 June, 2015). The starting date of this time window is set by the mission operation date of the *Fermi*-LAT, and the ending date by the time of analyses.

3.3 HE Gamma-ray Data

High-energy γ-ray (100 MeV $-$ 500 GeV) observations of Cen A that were contemporaneous to the *Swift*-BAT data, from the *Large Area Telescope* (LAT), the primary instrument on board the *Fermi gamma-ray Space Telescope* (*Fermi*) [21], were used to extract the γ-ray light curve. We employed the publicly available *Fermi*-LAT Pass 8 production [22], which has been optimized for point-like sources after a comprehensive review of γ-ray event analysis. Released in 2015, Pass 8 is considered to be the event reconstruction and analysis realizing the full scientific potential of the instrument by increasing the effective area, improving the point spread function, and widening the energy range that LAT is sensitive to. We performed unbinned analysis in the pylikelihood package of *Science Tools (v10r0p5)* to obtain the light curve in the energy range 0.1 to 500 GeV within 10° *region of interest* centered at the position of Cen A. In cases of small number of events per bin (e.g., when far away from the Galactic plane), LAT recommends the usage of unbinned analysis for time series data.
Assuming Cen A as having an underlying log-parabolic spectrum, we utilized *P8R2_SOURCE_V6* as the instrument response functions, while *gtmktime* was used to select good observation time intervals of the spacecraft. The diffuse emission from our Galaxy was taken into account using the *gll_iem_v06.fits* model while *iso_P8R2_SOURCE_V6_v06.txt* was the appropriate model for background cosmic rays and diffuse extragalactic γ rays. The flux normalization of Cen A, the Galactic and isotropic templates, and nearby bright sources were freed in the analysis.

Figure 3 shows the X-ray and γ-ray light curves described above. The light curves span 6.8 years of observations sampled in 14 day bins.

4. Time-lag Analysis

4.1 The Discrete Correlation Function

When multiple frequency band light curves have been observed from a source for a sufficiently long time, then the natural question is if these signals are in any way correlated. This question was answered traditionally by performing some *correlation function* analysis. A method that avoids interpolation of the data in the process, and which also deals with spurious effects due to correlated errors, has been proposed by [23]. This time series analysis, called the *discrete correlation function* (DCF), is powerful in that it can even handle sparse and or unevenly sampled light curves. The DCF progressively iterates through time-lags and computes a *discrete correlation coefficient* for each lag.

[2]The publicly available monitor web page, http://swift.gsfc.nasa.gov/docs/swift/results/transients/, provides light curves for astrophysical sources observed with *Swift*-BAT.

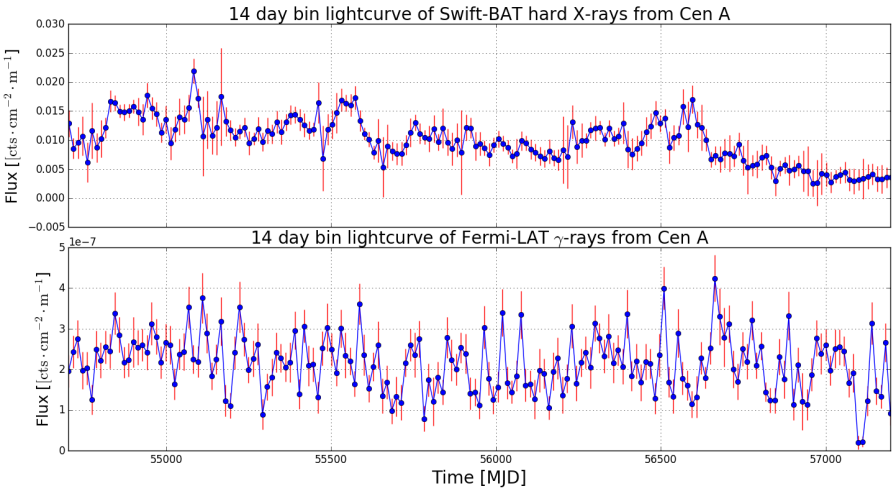

Figure 2: The *Swift*-BAT and *Fermi*-LAT light curves are shown here, where it can be clearly seen that the sampling of the X-rays in 14-day bins is much better over the *Fermi*-LAT binning.

This essentially means that each pair of points (one from each of the actual two light curves), gives one correlation value at a given lag. This enables an evaluation of the correlation between the two time series as a function of difference in arrival time of the signals. The result can be interpreted as trailing or leading of the first input signal if the lag is positive or negative, respectively.

4.2 Monte Carlo Simulation of Light Curves

In order to quantify the statistical significance of the DCF computed, we used the observed light curve in each band to simulate, via a Monte Carlo approach, 20 000 light curves. To accomplish this, an algorithm proposed by [24] and later improved by [25], was used. A Python implementation of this approach is published by [26].

For each observed light curve (the HE γ-ray and X-ray curves), we used the algorithm by [26] to extract the underlying *power spectral densities* (PSDs) and *probability density functions* (PDFs). These PSDs and PDFs are then used, also as implemented by [26], to simulate light curves that resemble the observations. In this way, we simulated two pairs of 20 000 light curves resembling the γ-ray and the X-rays, respectively. We then obtained correlation coefficients (using the [23] framework) by correlating each of the 20 000 simulated light curves against the other observed light curve. The simulated light curves feature the same variability and statistical properties as the observed light curves. These 20 000 simulated products were iteratively cross-correlated against the other observed waveband. For a given time lag, we sorted the correlation coefficients and determine the upper and lower 5% of these, from which we establish contour lines defined by the two outer boundaries containing 95% of the coefficients. These limits derived from the contour boundaries as the 95% *confidence level* of the DCF process is used as a statistical significance check of the correlations.

4.3 DCF Computation Result

Figure 3 shows the discrete correlation function between hard X-rays and HE γ rays of Cen A. This is essentially a plot of the correlation coefficient as a function of time-lag where the correlation was performed as described in Section 4.1. This distribution is approximately Gaussian for which the width is a measure of the uncertainty in the time lag. Overlaid on the correlation, is a band bounded by the 95% *confidence level* (see Section 4.2) which is surpassed by the peak of the correlation function. It can be noticed that the result hints to a scenario where the X-rays observed from the *Swift*-BAT instrument leads the *Fermi*-LAT γ-rays by 25 days (see the peak of the Gaussian fit which has a *standard deviation* of 152). The correlation coefficient at the peak is 0.35 ± 0.14. The result is established to have achieved over 95% confidence level using Monte Carlo simulations of light curves as described in Section 4.2.

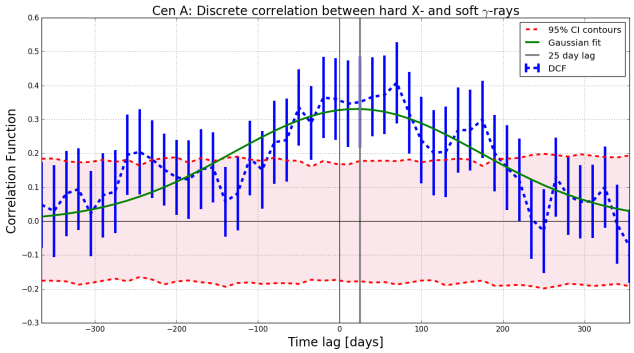

Figure 3: DCF result: The dotted blue curve denotes the DCF as a function of time-lag (with a overlaid green Gaussian fit), while the error bars on the correlation coefficients are propagated from the errors on the flux measurements. The peak at 25.0 day time lag (indicated by the solid gray vertical line), is the deduced time-lag by which HE γ-rays trail behind the X-rays. The reddish band is bounded by the 95% confidence contours. The lag bin width of the shown DCF is 15 days, constraint by the observation sampling rate and the duration of the observations. The latter also serves as a boundary to the lag range tested. This presented choice of the lag bin width and its range were arrived at by iterative visual inspection through these intervals.

5. Summary & Discussion

The light curve correlation between the 6.8 years of HE gamma-ray and the X-ray data of Cen A considered here, resulted in a *hint* of a possible time-lag of about 25 days of the gamma-ray emission behind the X-rays. The discrete correlation function (DCF) associated with this lag peaked at the value of 0.35 ± 0.14. Although the time-lag is a mere hint, the correlation is statistically significant beyond the 95% confidence level from Monte Carlo simulations of the light curves.

In the event that further studies confirms a time-lag of this magnitude, then we can couple that to arguments of light-travel time, to set a size constraint on the BLR of the system through

$$\begin{aligned} \Delta R &\sim c\ \Delta t_{\rm lag} \\ &\sim 6.5 \times 10^{16}\ {\rm cm} \end{aligned}$$

This would then indicate that the size of the BLR near the central engine is about 0.02 parsec. This estimate has considered the fact that we neglect *relativistic beaming* for a typical radio galaxy for which the jet is largely misaligned to our line of sight.

Acknowledgements

This project is sponsored by the German Academic Exchange Service (DAAD) (German: *Deutscher Akademischer Austauschdienst*), the *National Research Foundation*[3](NRF) and the *Department of Science and Technology* of the Republic of South Africa through the South African Research Chair Initiative under SARChI grant 64798, as well as the *Department of Physics* of the *University of Namibia*.

References

[1] Roustazadeh, P. & Boettcher, M., *Compton and Synchrotron Emission from Pair Cascades in Radio Galaxies*, AAS/High Energy Astrophysics Division, **12**, 4.08, (2011).

[2] Böttcher, M. & Els, P., *Gamma-Gamma Absorption in the Broad Line Region Radiation Fields of Gamma-Ray Blazars*, ApJ, **821**, 102-106, 2016.

[3] Fabian, A. C., Rees, M. J., Stella, L. & White, N. E., *X-ray fluorescence from the inner disc in Cygnus X-1*, MNRAS, **238**, 729-736, (1989).

[4] Israel, F. P., *Centaurus A - NGC 5128*, Astronomy & Astrophysics Review, **8**, 237-278, (1998).

[5] Marconi, A., Pastorini, G., Pacini, F., Axon, D. J., Capetti, A., Macchetto, D., Koekemoer, A. M. & Schreier, E. J., *The supermassive black hole in Centaurus A: a benchmark for gas kinematical measurements*, AAP, **448**, 921-953, (2006).

[6] Häring-Neumayer, N., Cappellari, M., Rix, H.-W., Hartung, M., Prieto, M. A., Meisenheimer, K. & Lenzen, R., *VLT Diffraction-limited Imaging and Spectroscopy in the NIR: Weighing the Black Hole in Centaurus A with NACO*, ApJ, **643**, 226-237, (2006).

[7] Fanaroff, B. L. & Riley, J. M., *The morphology of extragalactic radio sources of high and low luminosity*, MNRAS, **167**, 31P-36P, (1974).

[8] Graham, J. A., Brown, A. M., Boehm, C., Lacroix, T., Chadwick, P. M., & Joseph, S., *The Fermi-LAT spectrum of Centaurus A - Analysis and interpretations*, AIP Conference Proceedings, **1792**, 050004, (2017).

[9] Abdalla, H., Abramowski, A. & Aharonian, F. et al. (for the H. E. S. S. Collaboration), *The γ-ray spectrum of the core of Centaurus A as observed with H.E.S.S. and Fermi-LAT*, ArXiv e-prints, **1807.07375**, (2018).

[10] Abdo, A. A, Ackermann, M., & Ajello, M. et al. (for the Fermi-LAT Collaboration), *Fermi Large Area Telescope View of the Core of the Radio Galaxy Centaurus A*, ApJ, **719**, 1433-1444, (2010).

[11] Georganopoulos, M, & Kazanas, D., *Decelerating Flows in TeV Blazars: A Resolution to the BL Lacertae-FR I Unification Problem*, ApJL, **594**, L27 (2003).

[3]Disclaimer: Any opinion, finding and conclusion or recommendation expressed in this material is that of the authors and the NRF does not accept any liability in this regard.

[12] Petropoulou, M., Lefa, E., Dimitrakoudis, S. & Mastichiadis, A., *One-zone synchrotron self-Compton model for the core emission of Centaurus A revisited*, AAP, **562**, A12, (2014).

[13] Böttcher, M., Reimer, A., Sweeney, K. & Prakash, A., *Leptonic and Hadronic Modeling of Fermi-detected Blazars*, ApJ, **768**, 54, (2013).

[14] Fraija, N., Marinelli, A., Galván-Gámez, A. & Aguilar-Ruiz, E., *Modeling the spectral energy distribution of the radio galaxy IC310*, Astroparticle Physics, **89**, 14-22, (2017).

[15] Protheroe, R. J. & Biermann, P. L., *Photon-photon absorption above a molecular cloud torus in blazars*, Astropart. Physics, **6**, 293-300, (1997).

[16] Bernlöhr, K., Carrol, O., Cornils, R., Elfahem, S., Espigat, P., Gillessen, S., Heinzelmann, G., Hermann, G., Hofmann, W., Horns, D., Jung, I., Kankanyan, R., Katona, A., Khelifi, B., Krawczynski, H., Panter, M., Punch, M., Rayner, S., Rowell, G., Tluczykont, M. & van Staa, R., *The optical system of the H.E.S.S. imaging atmospheric Cherenkov telescopes. Part I: layout and components of the system*, Astropart. Physics, **20**, 111-128, (2003).

[17] Cornils, R., Gillessen, S., Jung, I., Hofmann, W., Beilicke, M., Bernlöhr, K., Carrol, O., Elfahem, S., Heinzelmann, G., Hermann, G., Horns, D., Kankanyan, R., Katona, A., Krawczynski, H., Panter, M., Rayner, S., Rowell, G., Tluczykont, M. & van Staa, R., *The optical system of the H.E.S.S. imaging atmospheric Cherenkov telescopes. Part II: mirror alignment and point spread function*, Astropart. Physics, **20**, 129-143, (2003).

[18] Gehrels, N., Chincarini, G., & Giommi, K.O., et al (for the Swift Sciebce Team) *The Swift Gamma-Ray Burst Mission*, ApJ, **611**, 1005-1020, (2004).

[19] Krimm, H. A., Barthelmy, S. D., Markwardt, C. B., Sanwal, D., Tueller, J., Gehrels, N. & Swift/BAT Team, *The Swift-BAT Hard X-ray Transient Monitor*, Bulletin of the American Astronomical Society, **38**, 374, (2006).

[20] Krimm, H. A., Holland, S. T., Corbet, R. H. D., Pearlman, A. B., Romano, P., Kennea, J. A., Bloom, J. S., Barthelmy, S. D., Baumgartner, W. H., Cummings, J. R., Gehrels, N., Lien, A. Y., Markwardt, C. B., Palmer, D. M., Sakamoto, T., Stamatikos, M. & Ukwatta, T. N., *The Swift/BAT Hard X-Ray Transient Monitor*, ApJSS, **209**, 14, (2013).

[21] Atwood, W. B., Abdo, A. A., & Ackermann, et al., *The Large Area Telescope on the Fermi Gamma-Ray Space Telescope Mission*, ApJ, **697**, 1071-1102, (2009).

[22] Atwood, W., Albert, A., Baldini, L., Tinivella, M., Bregeon, J., Pesce-Rollins, M., Sgrò, C., Bruel, P., Charles, E., Drlica-Wagner, A., Franckowiak, A., Jogler, T., Rochester, L., Usher, T., Wood, M., Cohen-Tanugi, J. & Zimmer, S. (for the Fermi-LAT Collaboration), *Pass 8: Toward the Full Realization of the Fermi-LAT Scientific Potential*, ArXiv e-prints 1303.3514, (2013).

[23] Edelson, R. A. & Krolik, J. H., *The discrete correlation function: A new method for analyzing unevenly sampled variability data*, ESA Special Publication, **281**, 646-659,(June 1988)

[24] Timmer, J. & Koenig, M., *On generating power law noise*, AAP, **300**, 707, (1995).

[25] Emmanoulopoulos, D., McHardy, I. M. & Papadakis, I. E., *Generating artificial light curves: revisited and updated*, MNRAS, **433**, 907-927, (2013).

[26] Connolly, S., *A Python Code for the Emmanoulopoulos et al. [arXiv:1305.0304] Light Curve Simulation Algorithm*, ArXiv e-print 1503.06676, (2015).